



# Effect of Lobe Count and Lobe Length of Corrugated Lobed Nozzle on Subsonic Flow Characteristics

V. P. Roy<sup>1</sup>, K. G. Kriparaj<sup>1,2,†</sup>, P. S. Tide<sup>1</sup> and N. Biju<sup>1</sup>

<sup>1</sup> School of Engineering, Cochin University of Science and Technology, Kochi – 682022, Kerala, India

<sup>2</sup> K. M. School of Marine Engineering, Cochin University of Science and Technology, Kochi – 682022, Kerala, India

†Corresponding Author Email: [kriparajkg@cusat.ac.in](mailto:kriparajkg@cusat.ac.in)

(Received April 25, 2022; accepted October 11, 2022)

## ABSTRACT

The corrugated lobed nozzle is an emerging research topic in jet flow dynamics, and little investigation has been conducted on its effect on flow characteristics. Thus, in this study, the effects of lobe count and lobe length of corrugated lobed nozzles on subsonic jet characteristics were experimentally investigated by analyzing the velocity profiles of the jets emanating from the nozzles. The Pitot tube readings were obtained by varying the count ( $4 \leq N \leq 8$ ) and length ( $10 \text{ mm} \leq L \leq 20 \text{ mm}$ ) of corrugated lobes. These measurements were then compared with the experimental readings obtained for a baseline circular nozzle. The nozzle pressure ratio (NPR) and exit nozzle area were kept identical at 1.5 and  $600 \text{ mm}^2$ , respectively, for all nozzle configurations. The most striking observation was the 'W'-shaped radial velocity profile of the corrugated nozzle, which differed from the 'Top hat' profile of the baseline circular nozzle. Additionally, the length of the potential central region of the corrugated nozzle was always shorter than that of the baseline circular nozzle, indicating the early occurrence of turbulence in the former. It was found that the lobe length had a meagre effect on the velocity variation in the jet issuing from the corrugated nozzle, whereas the lobe count had a significant effect on the velocity profile. However, as the lobe count increased, the velocity profile of the corrugated nozzle gradually resembled that of the circular nozzle. The findings of this study would be beneficial for selecting a proper lobe count and lobe length while designing and implementing a corrugated lobed nozzle.

**Keywords:** Corrugation; Jet; Lobe; Pitot tube; Velocity profile.

## NOMENCLATURE

$D$	diameter of the circular nozzle	$X$	distance measured in x-direction (Axial)
$L$	lobe length	$Y$	distance measured in y-direction (Radial)
$N$	lobe count	$Z$	distance measured in z-direction (Radial)
$P$	static pressure of the fluid	$\gamma$	ratio of specific heats
$P_o$	stagnation pressure of the fluid	$\rho$	static density of the fluid
$U$	velocity at a point	$\rho_o$	stagnation density of the fluid
$U_j$	maximum jet velocity		

## 1. INTRODUCTION

Typically, a nozzle is employed to develop a high-velocity jet because of its ability to convert potential energy into kinetic energy. Thus, it is inevitably used in various equipment, such as injectors, rockets, and airplanes. Therefore, research has been conducted on nozzle profiles as the simple modification of the nozzle profile itself can produce fascinating results in the aerodynamics of a jet arising from a nozzle.

Zaman *et al.* (2003) revealed that a reasonable increase in the lobe count of a rectangular lobed nozzle could reduce the noise; however, an excessive increase did not result in any additional noise suppression. Dawei *et al.* (2016) found that the addition of spoilers to a lobed nozzle could avoid high-temperature jet mixing. They also noted a decrease in the tube wall temperature owing to spoiler usage in the nozzle. Kopiev *et al.* (2013) evaluated the noise levels in a slightly corrugated nozzle and claimed that a noise reduction of 2.3 dB

was obtained, which was higher than that obtained by a circular nozzle. An experimental investigation on three-stream high-speed jets from a coaxial nozzle has been carried out by Papamoschou *et al.* (2014), who stated that at a low bypass ratio, coaxial nozzles produced no substantial noise reduction as compared to that produced by a single stream. Bühler *et al.* (2014) evaluated the acoustics of laminar and turbulent nozzle jet flows and found that the laminar and transitional exit conditions strongly enhanced the sound pressure levels.

Yang *et al.* (2012) investigated conical, elliptical, rectangular, square, and cross nozzles to understand the effect of the nozzle profile on the turbulence enhancement in a steam ejector. It was observed that the mixing process improved when the entrainment ratio was increased. Chong *et al.* (2014) conducted experimental and numerical investigations of a supersonic air ejector to identify the influence of geometrical factors and operation parameters on the flow field. The axisymmetric line static pressure and static wall pressure were constant in the critical mode, whereas an increase in these quantities has been observed with increasing discharge pressure in the subcritical mode. Hu *et al.* (2000, 2002) performed experimental investigations on lobed jet using planar laser-induced fluorescence (PLIF) and particle image velocimetry (PIV) illustrating the early appearance of a turbulent structure, development of spanwise Kelvin–Helmholtz vortices, and an intensive mixing region in the flow regime.

Tide and Srinivasan (2009) compared bevel and asymmetric chevron nozzles and observed that the latter had a better acoustic benefit. On further investigation of the chevron nozzles, Tide and Srinivasan (2010) found that a low penetration with a high chevron count resulted in maximum noise reduction. Mubarak and Tide (2018a) observed an enhanced thrust in a double parabolic nozzle as compared to that of a conical nozzle. Furthermore, Mubarak and Tide (2018b) found that the variations in the shock cell, potential core, and supersonic core lengths of the bell, double parabolic, and conical nozzles were negligible.

Callender *et al.* (2010) investigated the effects of serrated chevrons on the jet flow issuing from a coaxial circular nozzle. They reported that the chevrons effectively redistributed the momentum of the flow by developing sidewise jets, causing a fast decay rate of the jet velocity and inducing a reduction in the potential core region. De Gregorio (2014) investigated the effect of nozzle pressure ratio at an exit Mach number of 1.5 for under-expanded, correctly expanded, and over-expanded jet conditions. The axial Mach decay and spreading rates have been connected with flow structures and compressibility effects. Tam *et al.* (2008) conducted four types of experimental measurements for jet noise analysis and observed that fine-scale turbulent and large turbulent structures were the primary sources of jet noise. A numerical investigation of the corrugated lobed nozzle has been carried out by Paul *et al.* (2020a); they found that its potential core was lower than that of a circular nozzle. Moreover,

Kriparaj *et al.* (2022a) analyzed schlieren images of underexpanded flows from a lobed nozzle and found that a four-lobed nozzle resulted in an azimuthally varying shock net. A detailed study of azimuthally varying shock net based on varying nozzle pressure ratios was performed by Kriparaj *et al.* (2022b) and explored the shock net formation due to the interaction of peripheral and core shock waves developed from a corrugated lobed nozzle.

Although many studies have been conducted on different nozzles, the corrugated nozzle is a recent development in nozzle-jet flows. The significant parameters of a corrugated lobed nozzle are the lobe length and count, which may affect the flow characteristics of the jet. No structured experimental research has been conducted on corrugated lobed nozzles to determine their effect on subsonic jet dynamics. Thus, in this study, we investigated the velocity variation in the jet issuing from corrugated nozzles at different locations by varying the count ( $4 \leq N \leq 8$ ) and length ( $10 \text{ mm} \leq L \leq 20 \text{ mm}$ ). Furthermore, we compared the experimental data obtained for the corrugated nozzle with those of the baseline circular nozzle.

## 2. EXPERIMENTAL METHODOLOGY

A schematic of the free jet facility employed in this study is shown in Fig. 1 (Paul *et al.*, 2020b). It consisted of two tanks of  $14 \text{ m}^3$  and  $7 \text{ m}^3$  capacities, each with a maximum compressed air storage pressure of 30 bar. A three-stage reciprocating air compressor was used to fill the tank. To remove humidity, the compressed air was allowed to reach a settling chamber through a drier. A threaded nozzle holder was attached to the settling chamber, wherein different nozzles were attached. We employed the Pitot tube to obtain the readings at different points of the jet emerging from the nozzle using a three-axis traverse mechanism. The Pitot tube is a common flow-measuring device used to calculate the velocity of the fluid flow. It works on the principle that, owing to the right-angle bend of the Pitot tube, the velocity of the flow at a point would become zero (known as the stagnation point of the flow). This would then increase the pressure energy of the flow (owing to

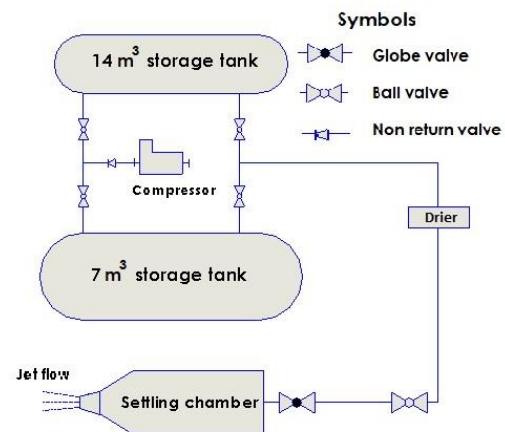


Fig. 1. Schematic of the free jet facility.

the conversion of kinetic energy into potential energy), which would be measured using pressure sensors attached to the tube.

For a compressible flow measured using a Pitot tube, the velocity and pressures were correlated by the compressible Bernoulli equation given by Eq. (1).

$$\frac{\gamma}{\gamma-1} \frac{P}{\rho} + \frac{U^2}{2} = \frac{\gamma}{\gamma-1} \frac{P_o}{\rho_o} \quad (1)$$

Here  $P$  and  $P_o$  are the static and stagnation pressures of the fluid respectively, whereas  $\rho$  and  $\rho_o$  are the static and stagnation densities of the fluid. Also, the velocity of the fluid and ratio of the specific heats are notated as  $U$  and  $\gamma$  respectively.



**Fig. 2. Corrugated lobed nozzles with lobe counts,  $N = 4, 6,$  and  $8.$**



**Fig. 3. Corrugated lobed nozzles with lobe lengths,  $L = 10$  mm,  $15$  mm, and  $20$  mm.**

The corrugated lobed nozzles used in this study were made of brass. The lobe count ( $N$ ) is defined as the number of protrusions present in the nozzle exit plane, and the lobe length ( $L$ ) is defined as the length measured along the axis between the inlet and exit of the corrugations. Figs. 2 and 3 show the corrugated nozzles with lobe counts of 4, 6, and 8, and lengths of 10, 15, and 20 mm, respectively. The Pitot tube

readings were obtained for these nozzles, and the results were compared with those of the baseline circular nozzle. The nozzle pressure ratio (NPR) and exit nozzle area were kept identical at 1.5 and 600 mm<sup>2</sup>, respectively, for all nozzle configurations used in this study.

### 3. RESULTS AND DISCUSSION

The Pitot tube readings were obtained in the axial and radial directions for each nozzle and plotted separately. The variation in the velocity of the jet with the lobe count and lobe length was analyzed.

#### 3.1 Variation of velocity with lobe count ( $N$ )

The experiment was performed by varying the lobe count while keeping the other parameters constant (exit area of 600 mm<sup>2</sup>, lobe penetration of 10 mm, and lobe length of 15 mm). The Pitot tube readings were obtained for NPR = 1.5 for all nozzle configurations.

Figure 4 shows the axial velocity profiles of the corrugated nozzles with varying lobe counts and that of the baseline circular nozzle. The corrugated nozzles had a much smaller potential core length of ' $2D$ ' than that of the baseline circular nozzle, which was ' $5.5D$ '. The potential region of the corrugated nozzle is smaller than the baseline nozzle due to the enhanced circumferential length (crest and trough) which in turn increases the interaction with free air, inducing the early formation of turbulent structures. The turbulent structures enhance dissipation and consecutively reduce the length of the potential central region of the corrugated lobed nozzle. From the plot, it is evident that the trend in the decay of the velocity varied with the lobe count. As the lobe count increased, there was a slight increase in the length of the potential central region. This may be because of a reduction in the groove space, which decreased the momentum transfer and dispersion chances.

The profiles of the radial velocity of the corrugated lobed nozzles with varying lobe counts and that of the baseline circular nozzle are shown in Fig. 5. At  $X/D = 0.5$ , the radial profile revealed a major

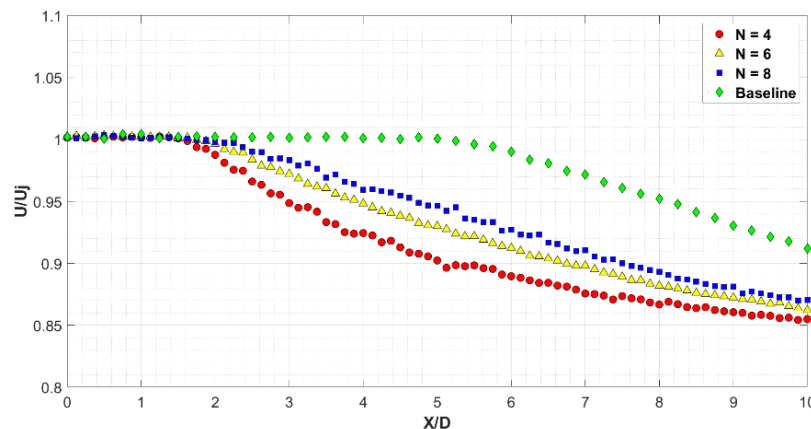


**Fig. 4. Axial velocity profiles of the baseline circular nozzle and corrugated lobed nozzles with different lobe counts.**

difference between the baseline circular and corrugated lobed nozzles. Owing to the presence of the lobes, there was a drop in the velocity in the middle of the profile at the lobed region, giving rise to a unique 'W'-shaped profile that deviated from the usual top hat profile of the circular nozzle. At  $X/D = 1$  and 2, the peak in the exterior lobe region gradually began to decrease and finally resembled the baseline circular nozzle profile as it proceeded downstream to  $X/D = 4$ . The peak value of the nozzles differed at  $X/D = 4$  owing to the change in the energy dissipation rate of each nozzle. It is evident from Fig. 4 that the four-lobed nozzle had the highest energy dissipation rate, followed by the six-lobed, eight-lobed, and baseline nozzles. Therefore, the peak value of the four-lobed nozzle was the lowest and that of the baseline nozzle was the highest at  $X/D = 4$ .

The axial contours of the velocity for the four, six, and eight-lobed corrugated nozzles are shown in Figs. 6–8, respectively. These contours differed from the parabolic contour of the circular nozzle because the lobed nozzles created a secondary peak level near the lobe. However, further downstream, these peaks dissolved rapidly, and only the centerline peak remained in the flow field. This rapid energy dissipation was due to the formation of small eddies in the vicinity of the grooved region. In addition, the

length of the potential central region increased corresponding to an increase in the lobe count. In Figs. 6 and 8, the four-lobed nozzle exhibited a feeble secondary peak compared to that of the eight-lobed nozzle. The four-lobed nozzle had a large trough region, which enabled the rapid energy dissipation of the jet emanating from the lobes. However, the eight-lobed nozzle exhibited a lower energy dissipation rate due to its smaller trough region, creating a much more predominant secondary peak.

The radial velocity contours of the corrugated lobed nozzles with different lobe counts are shown in Fig. 9; these contours assist in visualizing the section-wise velocity distribution of the nozzles. The yellow region in Fig. 9(a) indicates the potential core region of the four-lobed nozzle, which gradually decreased, as shown in Figs. 9(d) and 9(g). This demonstrates the dispersion tendency of the four-lobed nozzle. Even though the same level of velocity dispersion was seen for the six and eight-lobed nozzles, the effect of the lobes nearly disappeared at  $X/D = 4$ , as can be seen from their velocity contours in Figs. 9(h) and 9(i), respectively. Therefore, as the lobe count increased, the trends of the corrugated nozzles gradually resembled that of the circular nozzle owing to the decrease in the influence of the lobes.

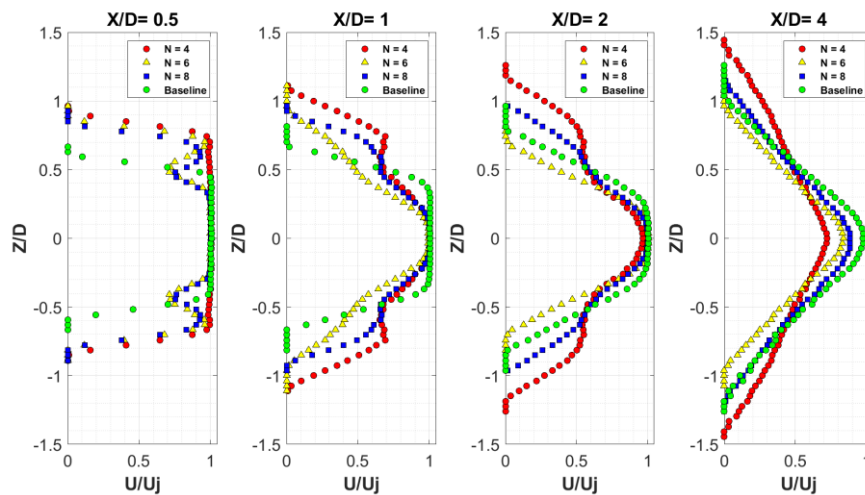


Fig. 5. Radial velocity profiles of the baseline circular nozzle and corrugated lobed nozzles with different lobe counts.

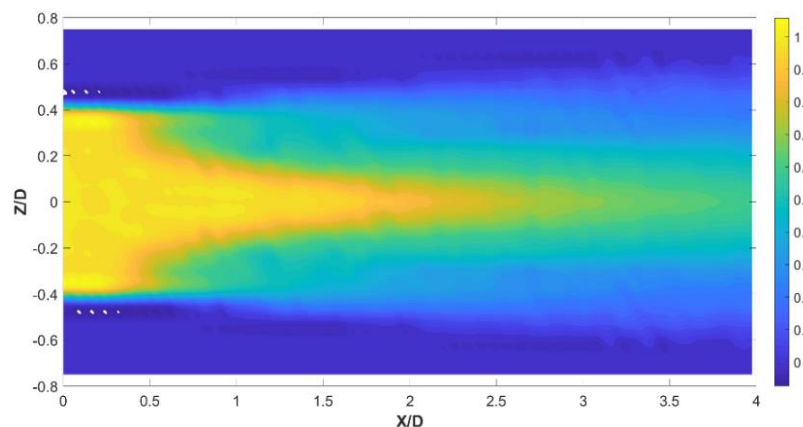
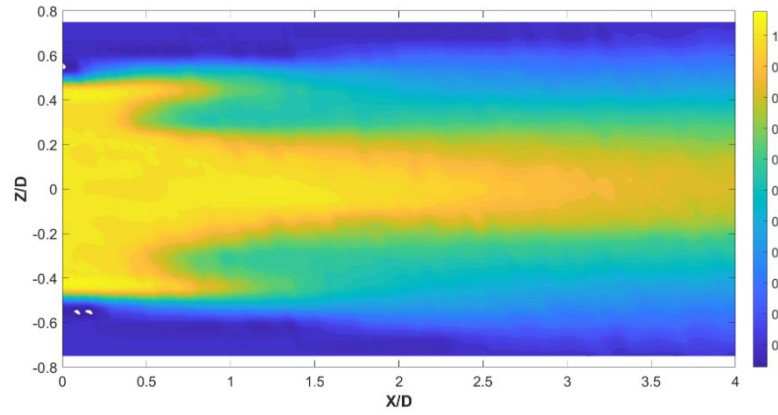
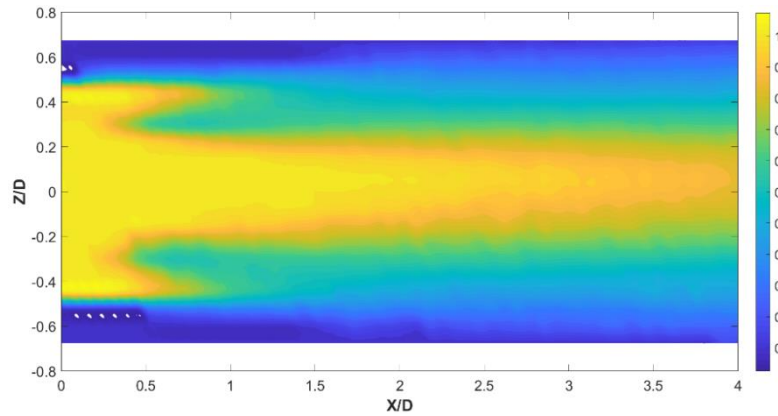


Fig. 6. Axial velocity contour of corrugated lobed nozzle with lobe count,  $N = 4$ .



**Fig. 7.** Axial velocity contour of corrugated lobed nozzle with lobe count,  $N = 6$ .



**Fig. 8.** Axial velocity contour of corrugated lobed nozzle with lobe count,  $N = 8$ .

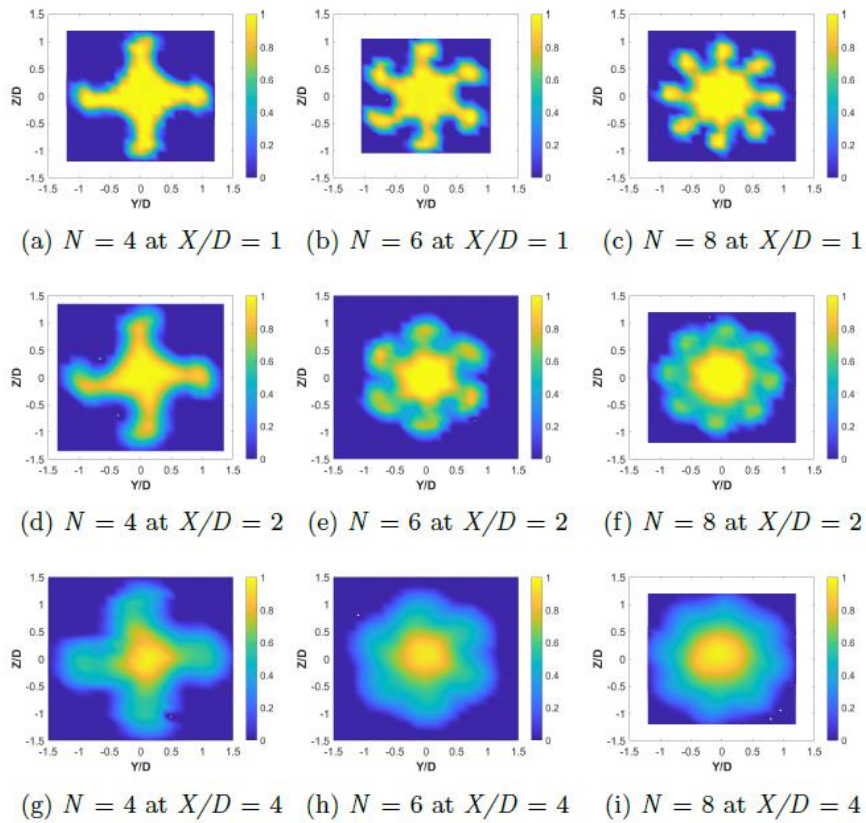


**Fig. 9.** Radial velocity contours of corrugated lobed nozzles with different lobe counts.

Moreover, the radial velocity profile shows a clockwise rotation of the flow owing to small-scale eddy formation, which was observed in all three nozzle configurations. The clockwise rotation may have been induced on the vortices owing to the Earth's rotational effect, especially along the Northern hemisphere. Therefore, the jet issuing from the corrugated nozzle would have a radial section-wise clockwise rotation along with an axial displacement of the fluid molecules.

Furthermore, in Fig. 9, at  $X/D = 4$ , the six and eight-lobed nozzles exhibited almost a similar pattern, whereas that of the four-lobed nozzle differed significantly. The four-lobed nozzle had a larger trough region as the lobes were placed at an angle of  $90^\circ$  from each other. This reduced the chances of interaction among the different jets emanating from the lobes. However, in the case of the six and eight-lobed nozzles, the angle of separation was much smaller than that of the four-lobed nozzle, which, in turn, increased the interaction among the different jets emerging from the lobes.

### 3.2 Variation of velocity with lobe length ( $L$ )

Three values of the lobe length, *i.e.*, 10, 15, and 20 mm, were considered to study its effect on the aerodynamics of jets issuing from the lobed nozzles, and the data were analyzed meticulously. The lobe count, nozzle exit area and penetration were kept identical as 4,  $600 \text{ mm}^2$ , and 10 mm, respectively; Pitot tube readings were obtained for  $\text{NPR} = 1.5$ .

The Pitot tube readings of the axial velocities for the corrugated lobed nozzles with different lengths of lobes from 10 mm to 20 mm with an increment of 5 mm, and those for the baseline circular nozzle are shown in Fig. 10. It is evident that the effect of the lobe length of the nozzle on the potential core was negligible. The values of the radial velocities for the corrugated lobed nozzles with varying lobe lengths and those for the circular nozzle are shown in Fig. 11. The profile of the corrugated nozzle at  $X/D = 0.5$  resembled the top-hat shape of the circular nozzle.

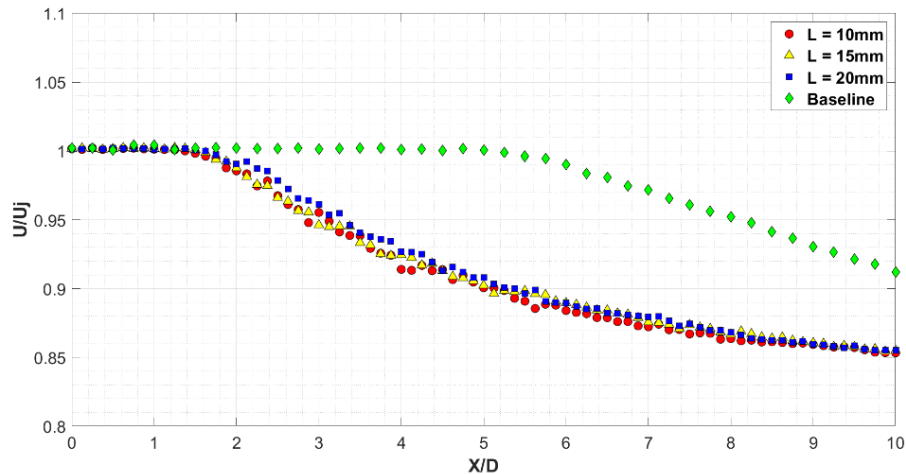


Fig. 10. Axial velocity profiles of the baseline circular nozzle and corrugated lobed nozzles with different lobe lengths.

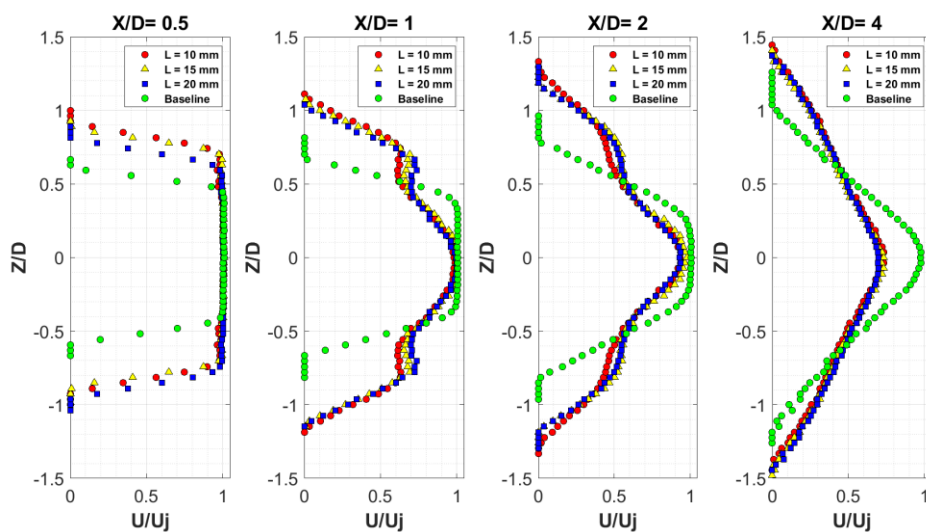
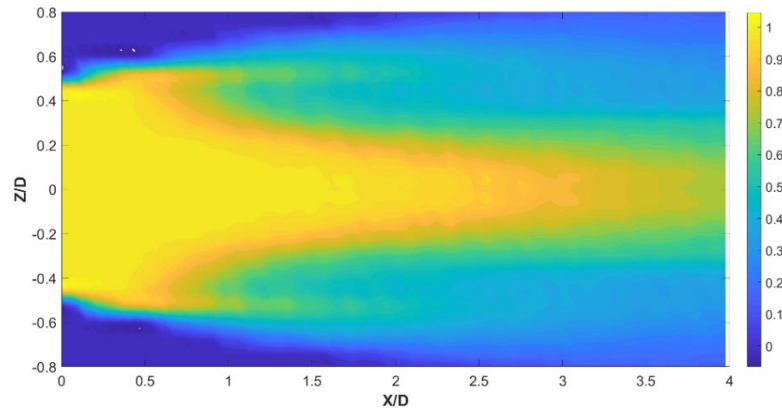
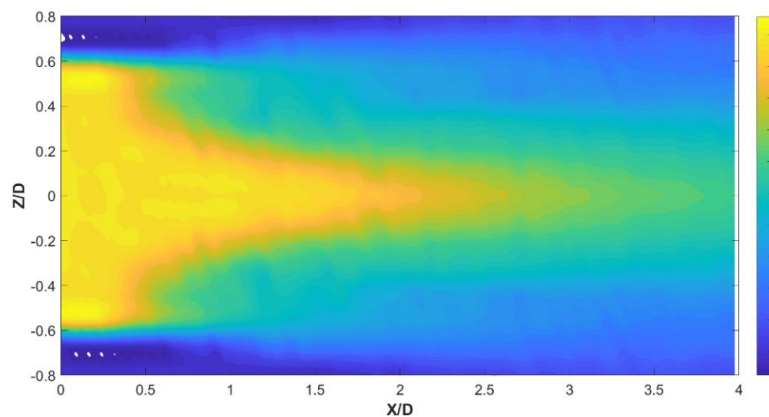


Fig. 11. Radial velocity profiles of the baseline circular nozzle and corrugated lobed nozzles with different lobe lengths.



**Fig. 12.** Axial velocity contour of corrugated lobed nozzle with lobe length  $L = 10$  mm.



**Fig. 13.** Axial velocity contour of corrugated lobed nozzle with lobe length  $L = 15$  mm.

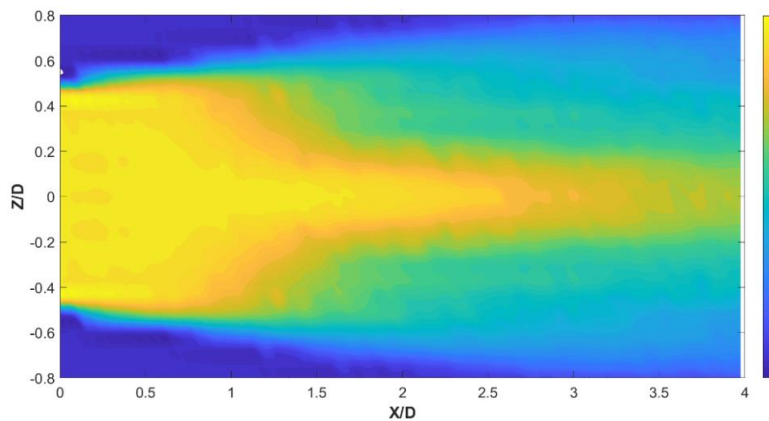


**Fig. 14.** Axial velocity contour of corrugated lobed nozzle with lobe length  $L = 20$  mm.

However, further downstream, the velocity profile became 'W'-shaped; this may be attributed to the rapid dissipation of energy of the jet from the small-scale structures formed in the groove space of the nozzle. The maximum velocity of the baseline circular nozzle was higher than those of the lobed nozzles at  $X/D = 4$ , whereas it was almost the same at other  $X/D$  values. This phenomenon was due to the enhanced dissipation rate exhibited by the corrugated lobed nozzle in comparison to that of the baseline circular nozzle. Thus, the energy of the lobed nozzle decreased drastically at  $X/D = 4$  compared with that of the baseline nozzle.

The axial velocity contours of the corrugated nozzles with the length of lobes such as 10, 15, and 20 mm are shown in Figs. 12-14, respectively. For all cases, the axial contours of the velocity were almost the same. Compared to the six and eight-lobed nozzles (Figs. 7 and 8), the four-lobed nozzles with different lobe lengths exhibited a weak hike along the exterior edge of the nozzle. This implies that the lobe count had a greater influence on the velocity profile than the lobe length. This can also be concluded from the radial velocity contours of the four-lobed nozzles with different lobe lengths, shown in Fig. 15; the contours were similar to each other at the same axial

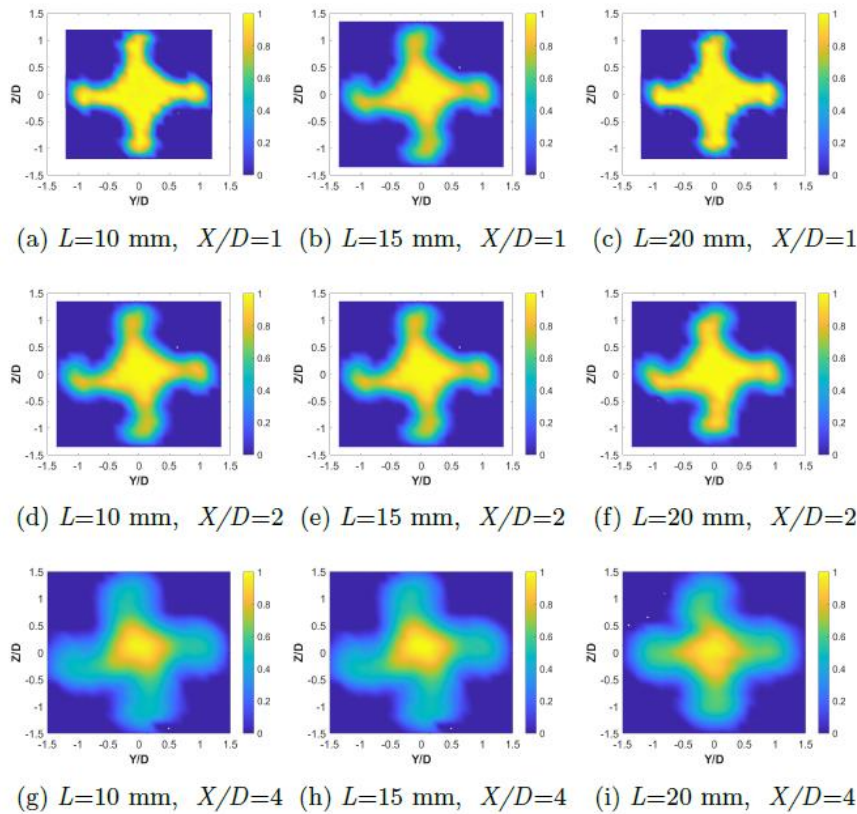


**Fig. 15. Radial velocity contours of corrugated lobed nozzles with different lobe lengths.**

position for all lobe lengths. The rotational effect induced by the lobes showed a similar trend in all three cases. The influence of lobe length variation on the aerodynamic characteristics of the jet was found to be negligible as the nozzle was convergent, and a positive pressure gradient was present inside it.

#### 4. CONCLUSION

Experiments were conducted on four, six, and eight-lobed corrugated nozzles, and the results obtained were compared with those of a circular nozzle. A significant deviation in the aerodynamic characteristics of the jet arising from the corrugated nozzles with a lower number of lobes was observed compared to those of the circular jets. This is because as the number of lobes increased, the space between the lobes decreased, and the nozzle area resembled a circular exit. Thereafter, experiments were performed for corrugated lobed nozzles with different lobe lengths, and the results obtained were compared with those of the baseline circular nozzle. The lobe length had a marginal influence on the velocity profile. However, a radial velocity profile with a 'W'-shape was evident in the case of the corrugated nozzle, which significantly differed from the 'Top hat' radial profile of the circular nozzle. The cross-sectional velocity contour exhibited a clockwise mode on the lobe-induced vortices owing to the Earth's rotational effect along the Northern Hemisphere. Thus, owing to the early formation of turbulent structures and increased energy dissipation rate in the case of a corrugated lobed nozzle, it would

be more suitable than a baseline nozzle for reducing the noise level of the jet and can be effectively used in the mixing of fluids. As the lobe length did not have a significant effect on the flow characteristics, it can be determined as per the cost of production. Additionally, a lobe count of four can be selected for the purpose of mixing, as it was found to produce a lower potential core than that produced by the other lobe counts.

#### REFERENCES

- Bühler, S., D. Obrist and L. Kleiser (2014). Laminar and turbulent nozzle-jet flows and their acoustic near-field. *Physics of Fluids* 26(8), 086103.
- Callender, B., E. J. Gutmark and S. Martens (2010). Flow field characterization of coaxial conical and serrated (chevron) nozzles. *Experiments in Fluids* 48(4), 637–649.
- Chong, D., M. Hu, W. Chen, J. Wang, J. Liu and J. Yan (2014). Experimental and numerical analysis of supersonic air ejector. *Applied Energy* 130, 679–684.
- Dawei, L., H. Jun, S. Zhiqiang and J. Jinzu (2016). The effects of spoilers on jet mixing of lobed nozzles. *Journal of Aerospace Technology and Management* 8(4), 459–466.
- De Gregorio, F. (2014). Free compressible jet investigation Application of laser techniques to fluid mechanics 2012. *Experiments in*

- Fluids* 55(3), 1–21.
- Hu, H., T. Saga, T. Kobayashi and N. Taniguchi (2000). Research on the vortical and turbulent structures in the lobed jet flow using laser induced fluorescence and particle image velocimetry techniques. *Measurement Science and Technology* 11(6), 698–711.
- Hu, H., T. Saga, T. Kobayashi and N. Taniguchi (2002). Mixing process in a lobed jet flow. *AIAA Journal* 40(7), 1339–1345.
- Kriparaj, K. G., R. V. Paul, P. S. Tide and N. Biju (2022a). An experimental study on shock cell structures of underexpanded jets from corrugated lobed nozzles using the schlieren imaging technique. *Journal of Flow Visualization and Image Processing* 29(4), 23–41.
- Kriparaj, K. G., R. V. Paul, P. S. Tide and N. Biju (2022b). Schlieren imaging investigation on azimuthally varying shock net from four-lobed corrugated nozzle. *Aircraft Engineering and Aerospace Technology* 94(7), 1058–1067.
- Kopiev, V. F., M. Y. Zaytsev and N. N. Ostrikov (2013). Subsonic jet noise suppression by a corrugated nozzle. *Acoustical Physics* 59(2), 207–209.
- Mubarak, A. K. and P. S. Tide (2018a). Design of a double parabolic supersonic nozzle and performance evaluation by experimental and numerical methods. *Aircraft Engineering and Aerospace Technology* 91(1), 145–156.
- Mubarak, A. K. and P. S. Tide (2018b). Experimental and computational exploration of underexpanded jets from conical, bell and double parabolic nozzles. *International Review of Mechanical Engineering* 12(1), 33–41.
- Papamoschou, D., A. D. Johnson and V. Phong (2014). Aeroacoustics of three-stream high-speed jets from coaxial and asymmetric nozzles. *Journal of Propulsion and Power* 30(4), 1055–1069.
- Paul, R. V., K. G. Kriparaj and P. S. Tide (2020a). Numerical predictions of the flow characteristics of subsonic jet emanating from corrugated lobed nozzle. *Aircraft Engineering and Aerospace Technology* 92(7), 955–972.
- Paul, R. V., K. G. Kriparaj, P. S. Tide and N. Biju (2020b). Design and installation of supersonic free jet test facility with flow visualization. *International Journal on Engineering Applications* 8(6), 233–240.
- Tam, C. K. W., K. Viswanathan, K. K. Ahuja and J. Panda (2008). The sources of jet noise: experimental evidence. *Journal of Fluid Mechanics* 615, 253–292.
- Tide, P. S. and K. Srinivasan (2009, May). Aeroacoustic studies of beveled and asymmetric-chevron nozzles. *15th AIAA/CEAS Aeroacoustics Conference (30th AIAA Aeroacoustics Conference)*, Miami, Florida, 1–14.
- Tide, P. S. and K. Srinivasan (2010). Effect of chevron count and penetration on the acoustic characteristics of chevron nozzles. *Applied Acoustics* 71(3), 201–220.
- Yang, X., X. Long and X. Yao (2012). Numerical investigation on the mixing process in a steam ejector with different nozzle structures. *International Journal of Thermal Sciences* 56, 95–106.
- Zaman, K. B. M. Q., F. Y. Wang and N. J. Georgiadis (2003). Noise, turbulence, and thrust of subsonic freejets from lobed nozzles. *AIAA Journal* 41(3): 398–407.